Model Predictive Control Based on Linear Parameter-Varying Models of Active Magnetic Bearing Systems

ABDELRAHMAN MORSI[1,2], **HOSSAM SEDDIK ABBAS**[2,3], **SABAH MOHAMED AHMED**[1,2], **AND ABDELFATAH MAHMOUD MOHAMED**[1,2], (Life Senior Member, IEEE)

[1]Mechatronics and Robotics Engineering Department, Egypt Japan University of Science and Technology, Alexandria 21934, Egypt
[2]Electrical Engineering Department, Assiut University, Assiut 71515, Egypt
[3]Institute for Electrical Engineering in Medicine, University of Lübeck, 23558 Lübeck, Germany

Corresponding author: Abdelrahman Morsi (abdelrahman.morsi@aun.edu.eg)

ABSTRACT *Active magnetic bearing* (AMB) system has been recently employed widely as an ideal equipment for high-speed rotating machines. The inherent challenges to control the system include instability, nonlinearity and constricted range of operation. Therefore, advanced control technology is essential to optimize AMB system performance. This paper presents an application of *model predictive control* (MPC) based on *linear parameter-varying* (LPV) models to control an AMB system subject to input and state constraints. For this purpose, an LPV model representation is derived from the nonlinear dynamic model of the AMB system. In order to provide stability guarantees and since the obtained LPV model has a large number of scheduling parameters, the *parameter set mapping* (PSM) technique is used to reduce their number. Based on the reduced model, a terminal cost and an ellipsoidal terminal set are determined offline and included into the MPC optimization problem which are the essential ingredients for guaranteeing the closed-loop asymptotic stability. Moreover, for recursive feasibility of the MPC optimization problem, a slack variable is included into its cost function. The goal of the proposed feedback control system is twofold. First is to demonstrate high performance by achieving stable levitation of the rotor shaft as well as high capability of reference tracking without violating input and state constraints, which increases the overall safety of the system under disturbances effects. Second is to provide a computationally tractable LPVMPC algorithm, which is a substantial requirement in practice for operating the AMB system with high performance over its full range. Therefore, we propose an LPVMPC scheme with frozen scheduling parameter over the prediction horizon of the MPC. Furthermore, we demonstrate in simulation that such frozen LPVMPC can achieve comparable performance to a more sophisticated LPVMPC scheme developed recently and a standard NL MPC (NMPC) approach. Moreover, to verify the performance of the proposed frozen LPVMPC, a comparison with a classical controller, which is commonly applied to the system in practice, is provided.

INDEX TERMS Model predictive control, linear parameter-varying models, magnetic bearing systems, parameter set mapping, asymptotic stability.

I. INTRODUCTION

Active magnetic bearing (AMB) systems are used in verity of industrial high-speed rotating machines including linear induction motors, compressors, flywheel storage systems,

The associate editor coordinating the review of this manuscript and approving it for publication was Bohui Wang.

wind turbines, etc. [1]–[3]. Moreover, AMB is used in medical applications, e.g., as a suspended rotor in ventricular assist devices for heart failure replacement in humans [4]. The electromagnetic forces generated in the AMB system provide contact-less suspension of its rotary component, which allows for very high rotational speeds without mechanical frictions.

The AMB is a multiple-input multiple-output (MIMO) highly nonlinear (NL) system. Its main control challenges are its inherent instability and the high coupling between the several controlled variables. The system is usually subject to vibrations, which complicates the controlling problem. Moreover, for safety of operation, it is necessary to incorporate the control system with constraints to cope with the limits of the inputs and states of the system. As an example, for safe operation, it is important to restrict movements of the rotor in the small air-gap, which separates it from the bearing, to specific limits even under disturbances, this can be achieved via state constraints. In order to tackle the difficulties of the AMB control system, PID [5], H_∞ [6] and Q-parametrization [7], [8] were proposed as linear controllers. NL controllers including feedback linearization [9], sliding mode control [10], and fuzzy control [11] also were considered. Moreover, several control techniques are proposed for the NL systems which can be applied onto the AMB system, e.g., [12], [13]. However, all these approaches cannot achieve safety in the sense of handling the system constraints.

Model predictive control (MPC) [14] is multivariable control strategy of many industrial applications [15], [16]. The MPC paradigm offers a unique ability to handle input/state constraints and to deal efficiently with time delay, instability, nonminimum phase, model mismatch disturbances and measurement noise. Moreover, it can optimize performance by iteratively solving online a constrained optimization problem based on predictions of the future behavior of the system over a so-called the prediction horizon N. For *linear time-invariant* (LTI) systems, the optimization problem can be solved efficiently online as a quadratic programming (QP) [17], whereas, for NL systems, it should be solved as a NL programming, which is very difficult to be implemented in practice. A promising approach to cope with that is to use *linear parameter-varying* (LPV) modeling framework [18] for describing NL models using linear representations dependent on a so-called scheduling parameter p, which is used for embedding nonlinearties of the system [19]. When the scheduling parameter is frozen, the LPV model can be seen as an LTI model according to the value of the frozen scheduling parameter. Therefore, MPC based on LPV models can be solved as a QP problem [20], which allows the MPC based on QP solvers for NL systems.

In the literature, MPC has been considered to control the AMB system, see, [21]–[24]; however, most of designed approaches were based on LTI models of the system. Therefore, optimal performance and stability can only be guaranteed locally as linear MPC (LMPC) strategy cannot deal efficiently with the nonlinearity of the system.

In this work we consider an experimental setup of an AMB system [25], see Fig. 1, and our goal is to design an efficient controller for the system which can deal with the challenges discussed above. Moreover, it can handle the input and state constraints and provide high performance with stability guarantees of the closed-loop system which are essential for safe operation. To achieve this goal, we propose

MPC based on LPV models (LPVMPC). To implement the LPVMPC, first, a NL model of the system is obtained. Then, it is converted into an LPV representation. The large number of the scheduling parameters of the derived LPV model renders the computations for establishing stability guarantees of the proposed closed-loop system intractable. To overcome such a difficulty, the *parameter set mapping* (PSM) based on *principle component analysis* (PCA) of [26] is used to reduce the number of the scheduling parameters.

For practical implementation of the MPC based LPV, we propose a frozen LPVMPC scheme, where, at every sampling time of the MPC problem, the scheduling parameter is frozen at its current value and over the prediction horizon. The main reason of this is that the future values of p, i.e., its values over the prediction horizon are unknown beforehand. However, such scheme, allows a single QP problem to be solved at every sample to obtain the optimal MPC control law. The computational burden is similar to that of the conventional LMPC; however, with a better performance for a wider range of operation. Such achievable control performance of the frozen LPVMPV is almost similar to that of NL MPC (NMPC) and iterative LPVMPC approaches. The latter has been developed recently in [27], where, at each sampling time the optimization problem is solved iteratively as a sequence of QP problems till convergence, which allows the scheduling parameter to be updated over the prediction horizon. This can enhance its achievable performance at the expense of extra computations for several QP problems per sample. Moreover, we include the MPC with a terminal cost and a terminal constraint set as an ellipsoidal invariant set, which are necessary ingredients to achieve asymptotic closed-loop stability [28], in addition to that, a slack variable is also included into the MPC to avoid infeasibility of the optimization problem.

To assess the performance of the frozen LPVMPC, we consider three control problems, regulation, reference tracking and disturbance rejection. We compare in simulation such frozen LPVMPC strategy with three different MPC approaches: the standard LMPC and two others more sophisticated techniques: the NMPC and the iterative LPVMPC. However, we show that the application of the frozen LPVMPC onto the AMB system can achieve comparable performance to both the NMPC and the iterative LPVMPC with simpler and practical implementation. Finally, in order to verify the performance of the frozen LPVMPC scheme in comparison with existent techniques in practice, a classical lead-lag controller developed by the manufacturer of the experimental setup AMB system [25] is considered.

The paper is organized as follows: Section II presents the NL model of the AMB system, which, is converted into an LPV form, then, the PSM method is applied to reduce the number of the scheduling parameters of the derived LPV model. The computations of the terminal ingredients for the MPC stability guarantees, its optimization problem as well as the design procedure for the different control problems considered in this work are discussed in Section III.

The simulation results are provided and illustrated in Section IV. Finally, the conclusion is presented in Section V.

II. MODELING OF THE AMB SYSTEM

A. THE NONLINEAR MODEL

The NL model of the AMB system, considered here, is based on the Magnetic Moments MBC500 experimental setup [25]. Its schematic diagram is shown in Fig. 1, the plant consists of a rotor which can be levitated using eight electromagnets, four at each end of the rotor. Hall-effect sensors are placed outside the electromagnets to measure the rotor displacement. The AMB system is a four degree of freedom (DOF) system with two DOF at each end of the rotor. The four DOF are translation in the horizontal direction (x_1 and x_2) and translation in vertical direction (y_1 and y_2), as shown in Fig. 1.
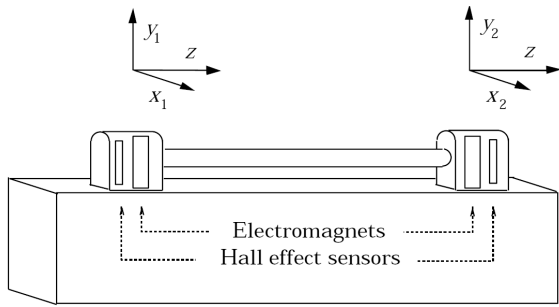

FIGURE 1. MBC500 system configuration [25].

Based on the geometry analysis of the rotor, the following expressions can be given

$$x_1 = x_0 - l_b \sin(\psi), \quad x_2 = x_0 + l_b \sin(\psi),$$
$$X_1 = x_0 - l_h \sin(\psi), \quad X_2 = x_0 + l_h \sin(\psi), \quad (1)$$
$$y_1 = y_0 - l_b \sin(\theta), \quad y_2 = y_0 + l_b \sin(\theta),$$
$$Y_1 = y_0 - l_h \sin(\theta), \quad Y_2 = y_0 + l_h \sin(\theta), \quad (2)$$

where the definitions of x_i, y_i, $i = 0, 1, 2$, X_j, Y_j, $j = 1, 2$, ψ and θ are given in Table 1; while the constant parameters l_b and l_h are defined in Table 2. Based on Newton's laws, the equations of motion governing the AMB system dynamics

TABLE 1. AMB system variables.

Symbol	Description
x_0 (y_0)	The horizontal (vertical) displacement of the center of mass of the rotor
x_1, x_2 (y_1, y_2)	The horizontal (vertical) displacements of the rotor at left and right bearing positions
X_1, X_2 (Y_1, Y_2)	The horizontal (vertical) displacements of the rotor at left and right Hall-effect sensor positions
θ	The pitch angle around the x axis
ψ	The yaw angle around the y axis
F_{x_1}, F_{x_2} (F_{y_1}, F_{y_2})	The horizontal (vertical) magnetic forces exerted on the rotor by left and right bearings
i_{x_1}, i_{x_2} (i_{y_1}, i_{y_2})	The horizontal (vertical) control currents applied on the rotor at left and right bearings
p_r	Rotation speed of the rotor

TABLE 2. AMB system parameters.

Symbol	Description	Value
L	Total length of the rotor	0.269 m
l_b	Distance from each bearing to the rotor center	0.1105 m
l_h	Distance from each Hall-effect sensor to the rotor center	0.1317 m
k_s	Electromagnetic constant	2.8×10^{-7} N.m²/Amp²
D_0	Nominal air-gap between the bearings and the rotor	0.0004 m
m	Mass of the rotor	0.2629 kg
g	Gravity of earth	9.81 m/s²
J_x	Moment of inertia of the rotor in the x direction	1.5884×10^{-3} kg.m²
J_z	Moment of inertia of the rotor in the z direction	5.05×10^{-6} kg.m²

are formulated as

$$m\ddot{x}_0 = F_{x_1} + F_{x_2}, \quad (3)$$
$$m\ddot{y}_0 = F_{y_1} + F_{y_2} - mg, \quad (4)$$
$$J_x\ddot{\psi} - p_r J_z\dot{\theta} = (F_{x_2} - F_{x_1})l_b \cos(\psi), \quad (5)$$
$$J_x\ddot{\theta} + p_r J_z\dot{\psi} = (F_{y_2} - F_{y_1})l_b \cos(\theta), \quad (6)$$

where the definitions of the variables $x_0, y_0, F_{x_1}, F_{x_2}, F_{y_1}, F_{y_2}$, ψ and θ are given in Table 1; the definitions and values of the constant parameters m, g, J_x, J_z, l_b are given in Table 2. Here, stationary rotor has been considered therefore, the rotation speed of the rotor $p_r = 0$. The generated electromagnetic force by each pair of electromagnets can be expressed as

$$F_{x_1} = k_s \left(\frac{(i_{x_1} + i_{bias_1})^2}{(x_1 - D_0)^2} - \frac{(i_{x_1} - i_{bias_1})^2}{(x_1 + D_0)^2} \right),$$

$$F_{x_2} = k_s \left(\frac{(i_{x_2} + i_{bias_1})^2}{(x_2 - D_0)^2} - \frac{(i_{x_2} - i_{bias_1})^2}{(x_2 + D_0)^2} \right),$$

$$F_{y_1} = k_s \left(\frac{(i_{y_1} + i_{bias_2})^2}{(y_1 - D_0)^2} - \frac{(i_{y_1} - i_{bias_1})^2}{(y_1 + D_0)^2} \right),$$

$$F_{y_2} = k_s \left(\frac{(i_{y_2} + i_{bias_2})^2}{(y_2 - D_0)^2} - \frac{(i_{y_2} - i_{bias_1})^2}{(y_2 + D_0)^2} \right), \quad (7)$$

see Table 1 for the definitions of $i_{x_1}, i_{x_2}, i_{y_1}, i_{y_2}$, the bias currents are $i_{bias_1} = 0.5$ Amp and $i_{bias_2} = 1$ Amp, and the constant parameter D_0 is given in Table 2. The values of ψ and θ for this system are very small, within ± 0.001 rad [25], therefore, we can assume that $\sin(\psi) \approx \psi$, $\sin(\theta) \approx \theta$ and $\cos(\psi) \approx 1$, $\cos(\theta) \approx 1$. To get the NL model of the system, we combine the equations (1)-(7). The resultant NL model has the inputs $i_{x_1}, i_{x_2}, i_{y_1}, i_{y_2}$, outputs X_1, X_2, Y_1, Y_2 and states $x_0, \dot{x}_0, y_0, \dot{y}_0, \psi, \dot{\psi}, \theta, \dot{\theta}$. Finally, the NL model of the AMB system (MBC500) can be expressed as

$$\dot{x} = f(x, u),$$
$$y = Cx + Du, \quad (8)$$

where

$$f(x, u) = \begin{bmatrix} \dot{x}_0 \\ (F_{x_1} + F_{x_2})/m \\ \dot{y}_0 \\ (F_{y_1} + F_{y_2} - mg)/m \\ \dot{\psi} \\ (F_{x_2} - F_{x_1})l_b/J_x \\ \dot{\theta} \\ (F_{y_2} - F_{y_1})l_b/J_x \end{bmatrix}, \tag{9}$$

and

$$C = \begin{bmatrix} 1 & 0 & 0 & 0 & -l_h & 0 & 0 & 0 \\ 1 & 0 & 0 & 0 & l_h & 0 & 0 & 0 \\ 0 & 0 & 1 & 0 & 0 & 0 & -l_h & 0 \\ 0 & 0 & 1 & 0 & 0 & 0 & l_h & 0 \end{bmatrix}, D = \begin{bmatrix} 0 \end{bmatrix}. \tag{10}$$

B. THE LPV MODELING

A continuous-time state-space LPV representation is given by

$$\begin{aligned} \dot{x} &= A(p)x + B(p)u + E(p), \\ y &= C(p)x + D(p)u, \end{aligned} \tag{11}$$

where $x \in \mathbb{R}^n$, $u \in \mathbb{R}^m$ and $y \in \mathbb{R}^p$, are the state, input and output vectors, respectively. The vector $E \in \mathbb{R}^n$ is an additive term, which includes factors that cannot be represented affinely on x or u. The system matrices $A \in \mathbb{R}^{n \times n}$, $B \in \mathbb{R}^{n \times m}$, $C \in \mathbb{R}^{p \times n}$, $D \in \mathbb{R}^{p \times m}$ and E depend on the scheduling parameter $p \in \mathbb{R}^q$ such that

$$p \in \mathcal{P}, \quad \mathcal{P} \subseteq \mathbb{R}^q,$$

where $\mathcal{P}$ is a compact set referred to as the parameter range and it is defined as

$$\mathcal{P} := \{p \in \mathbb{R}^q \mid p_{\min} \leq p \leq p_{\max}\},$$

with $p_{\min}$ and $p_{\max}$ represent componentwise the lower and upper bounds of p, respectively. Note that for representing NL models in the LPV representation (11); the scheduling parameter p often depends on the input, state or the output of the system, therefore, the LPV representation is referred in this case to as quasi-LPV form.

Next we describe the NL model (8) in the form of (11). This can be carried out by reformulating the NL equations (3)-(6) as follows

$$\begin{aligned} \ddot{x}_0 &= p_1 x_0 + p_2 \psi + p_9 i_{x_1} + p_{10} i_{x_2}, \\ \ddot{y}_0 &= p_3 y_0 + p_4 \theta + p_{11} i_{y_1} + p_{12} i_{y_2} + p_{17}, \\ \ddot{\psi} &= p_5 x_0 + p_6 \psi + p_{13} i_{x_1} + p_{14} i_{x_2}, \\ \ddot{\theta} &= p_7 y_0 + p_8 \theta + p_{15} i_{y_1} + p_{16} i_{y_2} + p_{18}, \end{aligned}$$

where $p_1, \ldots, p_{18}$ are the scheduling parameters. Such choice of the scheduling parameters yields the state-space matrices depend affinaly on them. Moreover, $p_1, \ldots, p_{18}$ are functions of the system states x_0, y_0, ψ, θ and the inputs $i_{x_1}, i_{x_2}, i_{y_1}, i_{y_2}$ as

$$p = f(v), \tag{12}$$

TABLE 3. Ranges of the scheduling parameters.

Parameter	Range	Parameter	Range
p_1	$(3.3 - 12.4) \cdot 10^4$	p_2	$0 - 9603.9$
p_3	$(8.2 - 36.9) \cdot 10^4$	p_4	$0 - 3 \times 10^4$
p_5	$0 - 1.6 \times 10^6$	p_6	$(6.7 - 25) \cdot 10^4$
p_7	$0 - 5 \times 10^6$	p_8	$(1.7 - 7.5) \cdot 10^5$
p_9	$13.3 - 22.1$	p_{10}	$13.3 - 265.9$
p_{11}	$19.9 - 33$	p_{12}	$19.9 - 397.1$
p_{13}	$-(404.1 - 243.5)$	p_{14}	$243.5 - 4863.4$
p_{15}	$-(603.5 - 363.6)$	p_{16}	$363.6 - 7263.1$
p_{17}	$5 - 26.7$	p_{18}	$0 - 468.5$

where $v \in R^s$, $s = 8$, which is referred to as the scheduling signal and $f : \mathbb{R}^s \to \mathbb{R}^q$ is a continuous mapping, $q = 18$; the functions f are given in Appendix A. The ranges of the scheduling parameters are determined based on their physical limits, we considered them as shown in Table 3, according to the system constraints that guarantee safe and stable operation of the AMB system. The state-space matrices of the LPV model for the AMB system are given as follows

$$A(p) = \begin{bmatrix} 0 & 1 & 0 & 0 & 0 & 0 & 0 & 0 \\ p_1 & 0 & 0 & 0 & p_2 & 0 & 0 & 0 \\ 0 & 0 & 0 & 1 & 0 & 0 & 0 & 0 \\ 0 & 0 & p_3 & 0 & 0 & 0 & p_4 & 0 \\ 0 & 0 & 0 & 0 & 0 & 1 & 0 & 0 \\ p_5 & 0 & 0 & 0 & p_6 & 0 & 0 & 0 \\ 0 & 0 & 0 & 0 & 0 & 0 & 0 & 1 \\ 0 & 0 & p_7 & 0 & 0 & 0 & p_8 & 0 \end{bmatrix}, \tag{13}$$

$$B(p) = \begin{bmatrix} 0 & 0 & 0 & 0 \\ p_9 & p_{10} & 0 & 0 \\ 0 & 0 & 0 & 0 \\ 0 & 0 & p_{11} & p_{12} \\ 0 & 0 & 0 & 0 \\ p_{13} & p_{14} & 0 & 0 \\ 0 & 0 & 0 & 0 \\ 0 & 0 & p_{15} & p_{16} \end{bmatrix}, \quad E(p) = \begin{bmatrix} 0 \\ 0 \\ 0 \\ p_{17} \\ 0 \\ 0 \\ 0 \\ p_{18} \end{bmatrix}. \tag{14}$$

The considered LPV system (11) is called the *affine* LPV representation as the state-space matrices (13) and (14) depend on the scheduling parameters in an affine manner. Note that, most of LPV based control approaches in the literature [29] consider affine LPV representations.

Including stability and feasibility conditions for the MPC is necessary to guarantee the convergence of the system state and the recursive feasibility of its optimization problem, i.e., if the optimization problem is initially feasible it remains feasible afterwards. The ingredients of these guarantees according to the framework of [28] are to add a terminal cost, commonly a quadratic cost, to the optimization problem of the MPC and to include a terminal constraint as an invariant set. The computations of the terminal cost and the terminal set are often performed offline; their complexity increases significantly with the order of the system and the number of the scheduling parameters in the LPV case.

There exist algorithms in the literature for computing these ingredients; however, due to the involved computational complexity, the application of most of these algorithms can be carried out for very simple 2nd- to 4th-order systems in simulation with one or two scheduling parameters in the LPV case [30], [31]. In contrast, with the system considered in this work, which is of 8th order and 18 scheduling parameters with affine dependence, computing the terminal cost and the terminal constraint set is intractable with available tools in the literature, e.g., [32], [33]. For example, to compute the terminal cost as a quadratic function of the states and the terminal constraint as an ellipsoid invariant set for the affine dependence case, one should solve a linear matrix inequality (LMI) optimization problem subject to $2^q = 2^{18}$ LMIs constraints, which is very complex. Therefore, to be able to provide stability guarantees of the proposed LPVMPC, we should reduce the number of the scheduling parameters without significantly affect the accuracy of the model. We use here the PSM approach of [26], which has proven its efficiency in several LPV practical applications [34].

C. PARAMETER SET MAPPING

PSM [26] is a systematic procedure to find tighter regions in the space of the scheduling parameters. Moreover, approximations of LPV models can be obtained which neglect insignificant directions in the mapped parameter space without ad-hoc model simplifications and parameter freezing and also without loosing much information about the plant. Using PSM allows a trade-off between the number of parameters and model accuracy in a straightforward way. This method is used in this paper to reduce the number of scheduling parameters of the obtained LPV model (11) to yield the computations of the terminal cost and the terminal set tractable.

In the following, we review the PSM approach. We aim at determining a mapping $h : \mathbb{R}^s \to \mathbb{R}^{\hat{q}}$, such that $\hat{q} < q$, and

$$\xi = h(v), \qquad (15)$$

that leads to an LPV model

$$\dot{x} = \hat{A}(\xi)x + \hat{B}(\xi)u + \hat{E}(\xi),$$
$$y = \hat{C}(\xi)x + \hat{D}(\xi)u, \qquad (16)$$

which can reasonably approximate the original model (11).

First, typical trajectories of the scheduling signals are generated, which cover the expected range of operation of the controlled plant. These trajectories are sampled at time instants $t = kT, k = 0, 1, \ldots, N_d - 1, N_d \gg q$. Next, the corresponding scheduling parameters are computed using (12) to construct the data matrix

$$P = [p(0) \, p(T) \, \ldots \, p((N_d - 1)T)] \in \mathbb{R}^{q \times N_d}, \qquad (17)$$

where its ith row P_i represents the trajectory of parameter p_i. To put the same weight on each p_i, all rows of P are normalized using an operation $\mathcal{N}_i$ such that each row has zero mean with unity standard deviation

$$P_i^n = \mathcal{N}_i(P_i) = (P_i - m_i)/c_i, \qquad (18)$$

$$P_i = \mathcal{N}_i^{-1}(P_i^n) = c_i P_i^n + m_i, \qquad (19)$$

where m_i, c_i are the mean and standard deviation of each row P_i, respectively. This results in a normalized data matrix $P^n = \mathcal{N}(P)$. Next, PCA [35] is applied to the normalized data by applying the a singular value decomposition on P^n as follows

$$P^n = \begin{bmatrix} U_s & U_n \end{bmatrix} \begin{bmatrix} \Sigma_s & 0 & 0 \\ 0 & \Sigma_n & 0 \end{bmatrix} \begin{bmatrix} V_s^T \\ V_n^T \end{bmatrix}, \qquad (20)$$

where $U_s \in \mathbb{R}^{q \times \hat{q}}$, $U_n \in \mathbb{R}^{q \times (q - \hat{q})}$, $\Sigma_s = \text{diag}(\sigma_1 \ldots \sigma_{\hat{q}})$, $\Sigma_n = \text{diag}(\sigma_{\hat{q}+1} \ldots \sigma_q)$, $V_s \in \mathbb{R}^{N_d \times \hat{q}}$ and $V_n \in \mathbb{R}^{N_d \times (N_d - \hat{q})}$. The matrices U_s, Σ_s, V_s correspond to the $\hat{q}$ significant singular values, such that

$$\hat{P}^n = U_s \Sigma_s V_s^T \approx P^n, \qquad (21)$$

is a reasonable approximation of the given data. To evaluate the accuracy of the approximated model, as suggested in [26], we use the ratio

$$v_m\% = \frac{\sum_{i=1}^{\hat{q}} \sigma_i^2}{\sum_{i=1}^{q} \sigma_i^2} \times 100, \qquad (22)$$

where σ_i denote the singular values in (20). The number $\hat{q}$ of scheduling parameters, can be used to balance the accuracy of the model against its complexity. The matrix U_s composes a basis for the significant column space of the data matrix P^n, and is used to determine a reduced mapping h (15) as follows

$$\Xi = U_s^T P^n \in \mathbb{R}^{\hat{q} \times N_d} \Rightarrow \xi = h(v) = U_s^T \mathcal{N}(f(v)). \qquad (23)$$

Finally, the approximate mappings $\hat{A}(\cdot), \hat{B}(\cdot), \hat{C}(\cdot), \hat{D}(\cdot)$ and $\hat{E}(\cdot)$ in (16) are related to (11) by

$$\begin{bmatrix} \hat{A}(\xi) & \hat{B}(\xi) & \hat{E}(\xi) \\ \hat{C}(\xi) & \hat{D}(\xi) & - \end{bmatrix} = \begin{bmatrix} A(\hat{p}) & B(\hat{p}) & E(\hat{p}) \\ C(\hat{p}) & D(\hat{p}) & - \end{bmatrix}, \qquad (24)$$

$$\hat{p} = \mathcal{N}^{-1}(U_s \xi)$$
$$= \mathcal{N}^{-1}(U_s U_s^T \mathcal{N}(f(v))), \qquad (25)$$

where $\mathcal{N}^{-1}$ denotes the re-scaling operation. At any given time, the reduced parameter vector ξ can be computed using (23), while the approximate LPV model can be obtained using (24) and (25).

We apply the PSM technique to the LPV model (11). Fig. 2 illustrates the plot of $v_m\%$ versus $\hat{q}$, where $\hat{q} = 3$ is chosen which reveals that 98% of the information is maintained. For better evaluation of the approximate models, we, first, compute the approximated data matrix $\hat{P}$ using (23) and (25) as follows

$$\hat{P} = \mathcal{N}^{-1}(U_s \Xi) = \mathcal{N}^{-1}(U_s U_s^T P^n), \qquad (26)$$

then, we compute the *best fit rate* (BFR)% between the actual and approximated data,

$$BFR_i\% = \max\left(0, 1 - \frac{\|P_i - \hat{P}_i\|}{\|P_i - m_i\|}\right) \times 100, \qquad (27)$$

where $i = 1, \ldots, q$, $\hat{P}_i$ is the ith row of the data matrix $\hat{P}$, which, represents the trajectories of the projected parameters
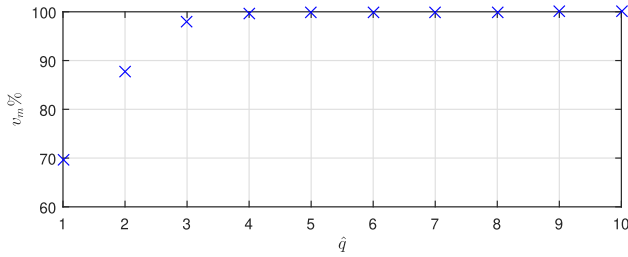
FIGURE 2. Fraction of total variation v_m% versus $\hat{q}$.

TABLE 4. *BFR* % between the actual and approximated scheduling parameters.

Parameters	BFR %	Parameters	BFR %
$p_1, \hat{p}_1$	87.7	$p_2, \hat{p}_2$	91
$p_3, \hat{p}_3$	82.9	$p_4, \hat{p}_4$	92.7
$p_5, \hat{p}_5$	91	$p_6, \hat{p}_6$	87.7
$p_7, \hat{p}_7$	92.7	$p_8, \hat{p}_8$	82.9
$p_9, \hat{p}_9$	96.3	$p_{10}, \hat{p}_{10}$	77.8
$p_{11}, \hat{p}_{11}$	88.8	$p_{12}, \hat{p}_{12}$	78
$p_{13}, \hat{p}_{13}$	96.3	$p_{14}, \hat{p}_{14}$	77.8
$p_{15}, \hat{p}_{15}$	88.8	$p_{16}, \hat{p}_{16}$	78
$p_{17}, \hat{p}_{17}$	91.3	$p_{18}, \hat{p}_{18}$	92.6

$\hat{p}_i$ on the reduced parameter space. Table 4 shows the values of the *BFR* % between the trajectories of p_i and $\hat{p}_i$, which indicate satisfactory approximation of the data.

Since MPC is adopted here, a discrete-time representation of the LPV model should be obtained. The rectangular (Euler's forward) method is used to discretise the state-space LPV model (11) of the system. Choosing an appropriate sampling time for this control system problem is challenging as it should accommodate the large bandwidth of the AMB system, which is 200 Hz; on the other hand, it should be large enough to be able to solve the optimization problem of the MPC. It turns out that choosing a sampling time of $T_s = 6.25 \times 10^{-4}$ s can compromise such conflict. Finally, we can write the discrete-time LPV model as:

$$x(k + 1) = A_d(p(k))x(k) + B_d(p(k))u(k) + E_d(p(k)),$$
$$y(k) = C_d x(k) + D_d u(k), \tag{28}$$

where

$$A_d(p(k)) = I_n + T_s A(p), \tag{29}$$
$$B_d(p(k)) = T_s B(p), \quad E_d(p(k)) = T_s E(p), \tag{30}$$
$$C_d = C, \quad D_d = D, \tag{31}$$

where $I_n \in \mathbb{R}^{n \times n}$ is the identity matrix, $A(p), B(p), E(p)$ are computed from (13) and (14), and C, D are given in (10).

III. CONTROL DESIGN
A. PROCEDURE
Before we illustrate the control design adopted here, we summarize the control design objectives and procedure of this work. Given the NL model (8) of the AMB system, the objective is to design a controller that can

- deal with the nonlinearity of the system,

- handle the input and state constraints,
- provide stability and feasibility guarantees.

Based on such NL model (8), the LPV representation (11) is derived, then, the PSM method of [26] is used to reduce the number of the scheduling parameters of the obtained LPV model to be able to perform the computations required for establishing stability guarantees. Thereafter, the MPC with stability and feasibility guarantees can be implemented online.

B. MODEL PREDICTIVE CONTROL
Here, we, first, demonstrate the MPC optimization problem used in this work. Then, we present the offline computations regarding the terminal cost and terminal constraint set which are used as stability guarantees for all the MPC schemes considered in this work.

In the considered MPC schemes, at every sampling instant $k \geq 0$, the following optimization problem is solved:

$$\min_{U(k),\, S_x(k)} J(k), \tag{32}$$

subject to

$$|u_j(k + i|k)| \leq u_{j,\max}, j = 1, \ldots, m,$$
$$|x_l(k + i|k)| \leq x_{l,\max} + S_{x_l}(k), l = 1, \ldots, n,$$

and

$$(\star)^T \Phi(x(k + N|k) - x_s) \leq \alpha,$$

where $J(k)$ is the cost function and $U(k)$ is a vector contains the whole control inputs over the prediction horizon N, which are among the decision variables of the optimization problem and can be written as:

$$U(k) = \begin{bmatrix} u(k|k) \\ u(k+1|k) \\ \vdots \\ u(k+N-1|k) \end{bmatrix},$$

and $S_x(k) \in \mathbb{R}^n$ is a slack variable used for softening the system state constraints, $u_j(k + i|k)$ and $x_l(k + i|k)$ are the control input j and state l, respectively, at the step i of the prediction horizon N at sampling time k. The upper limits of the control input j and state l are $u_{j,\max}$ and $x_{l,\max}$, respectively, $x_s \in \mathbb{R}^n$ is the steady-state vector, we will explain later how to compute x_s. The matrix $\Phi \in \mathbb{R}^{n \times n}$ and the scalar α are computed offline to build the terminal cost and the terminal set, respectively.

Using the slack variables relaxes the constraints when it is necessary to avoid infeasibility of the optimization problem. However, it should be used carefully so that it leads to realistic constraints relaxation agreed with the physical constraints. Note that, for physical systems, the input constraints depend on the actuator limits, therefore, they are not subject to any further relaxation and hence no slack variables are assigned for the input constraints. On the other hand, we allow a slight softening for the state constraints to

avoid infeasibility problem. That is justifiable as we consider during the normal operation more tightened state constraints for increasing safety. Then, when it is necessary, they can be shortly relaxed to an acceptable physical limit. Therefore, we incorporate the slack variable $S_x(k)$ in the optimization problem (32) for that purpose without harming the AMB system operation.

The cost function $J(k)$ is given as

$$J(k) = J_N(k) + J_{sv}(k) + J_\infty(k), \qquad (33)$$

where $J_N(k)$ is a quadratic stage cost function which is computed over the prediction horizon N, $J_{sv}(k)$ is used to minimize the slack variable $S_x(k)$ and $J_\infty(k)$ is the terminal cost.

The cost function $J_N(k)$ has two forms based on the considered control problem: regulation or reference tracking. For the regulation problem, it is given as

$$J_N(k) = \sum_{i=0}^{N-1} \star^T Q x(k+i|k) + \star^T R u(k+i|k), \qquad (34)$$

where $Q \in \mathbb{R}^{n \times n}$ and $R \in \mathbb{R}^{m \times m}$ are positive semi-definite and positive definite symmetric matrices, respectively. Choosing the appropriate values for Q and R is important for tuning control objectives, as, Q is used to set the speed of the state performance and R is used to penalize the control effort.

For the reference tracking problems $J_N(k)$ is given by

$$J_N(k) = \sum_{i=0}^{N-1} (\star)^T Q_y(r(k+i|k) - y(k+i|k))$$
$$+ (\star)^T R(u(k+i|k) - u_s), \qquad (35)$$

where $r(\cdot)$ is the reference trajectory, $Q_y \in \mathbb{R}^{p \times p}$ is a positive semi-definite symmetric matrix which is used to set the output performance and $u_s \in \mathbb{R}^m$ is the steady-state input vector corresponding to x_s, its computation will be presented later.

The cost function $J_{sv}(k)$ is computed as

$$J_{sv}(k) = S_x(k)^T Q_{s_x} S_x(k), \qquad (36)$$

where $Q_{s_x} \in \mathbb{R}^{n \times n}$ is positive semi-definite symmetric matrix which is used as weighting matrix for penalizing $S_x(k)$.

The terminal cost $J_\infty(k)$ is computed as

$$J_\infty(k) = (\star)^T \Phi(x(k+N|k) - x_s), \qquad (37)$$

where the matrix Φ is computed offline by solving the following feasibility LMI problems [27]

$$\begin{bmatrix} Y & \star^T & \star^T & \star^T \\ A(\hat{p})Y + B(\hat{p})X & Y & 0 & 0 \\ Y & 0 & Q^{-1} & 0 \\ X & 0 & 0 & R^{-1} \end{bmatrix} \geq 0, \qquad (38)$$

$$Y > 0, \qquad (39)$$

where $Y = Y^T \in \mathbb{R}^{n \times n}$, $X \in \mathbb{R}^{m \times n}$ are free decision variables, such that $\Phi = Y^{-1}$. The system matrices $A(\hat{p})$ and $B(\hat{p})$ are computed at every $\hat{p}$ obtained by (25) at each vertex computed using the min/max values of every row of

the reduced data matrix Ξ (23). Note that, in this paper, we choose the number of the reduced scheduling parameters (rows of Ξ) as $\hat{q} = 3$, by considering the min/max values of each row, we have 8 vertices, at which, $\hat{p}$ is calculated. That's why, we use the PSM method, as if we consider the actual number of scheduling parameter, which is $q = 18$, we would get 262144 vertices, which is a very complex problem. Therefore, with $\hat{q} = 3$, the LMI problem (38) is solved as a feasibility problem subject to 8 LMI constraints in addition to the constraint on the matrix Y (39).

To compute the scalar α of the ellipsoidal terminal set

$$(\star)^T \Phi(x(k+N|k) - x_s) \leq \alpha, \qquad (40)$$

given in (32), the following optimization problem [36] is solved:

$$\max_{\tilde{\alpha}} \tilde{\alpha}, \qquad (41)$$

subject to

$$\tilde{\alpha}^2 [A_f]_i \Phi^{-1} [A_f]_i^T \leq [b_f]_i^2, \quad i = 1, \dots, 2(n+m),$$

where $\tilde{\alpha} = \sqrt{\alpha}$, $A_f \in \mathbb{R}^{2(n+m) \times n}$ and $b_f \in \mathbb{R}^{2(n+m)}$ are given as

$$A_f = \begin{bmatrix} -I_n \\ F \\ I_n \\ -F \end{bmatrix}, \quad b_f = \begin{bmatrix} x_{\max} - x_s \\ u_{\max} \\ x_{\max} - x_s \\ u_{\max} \end{bmatrix}, \qquad (42)$$

where $F = X\Phi$, which is computed by (38) and it is usually referred to as the terminal controller [28]. Note that, α should be computed for every steady-state as b_f depends on x_s.

The computation of x_s and u_s depends on the desired reference value $r \in \mathbb{R}^p$, which should satisfy the following conditions:

$$u_s = (C_d(I_n - A_d)^{-1}B_d)^{-1}r,$$
$$x_s = (I_n - A_d)^{-1}B_d u_s, \qquad (43)$$

where C_d is given in (31), which is a constant matrix, however, A_d, B_d are dependent on x_s and u_s as well, see (29) and (30). Therefore, computing x_s and u_s for a given reference value is a matter of solving a nonlinear set of algebraic equations, which can be solved using any of the Newton methods for solving nonlinear equations [37]. The initial conditions can be changed to ensure that the solution satisfies the constraints $|x_s| \leq x_{\max}$ and $|u_s| \leq u_{\max}$. Otherwise, nonlinear optimization tools subject to constraints can be utilized. Note that, when a piecewise constant reference is considered, a pair of (x_s, u_s) should be obtained for each reference value.

By solving the optimization problem (32) and following the receding horizon principle, only the first element of $U(k)$, i.e., the vector $u(k|k)$, is applied onto the system. Note that, the same symbol $J_N(k)$ is used for both regulation (34) and reference tracking (35) problems, however, they will be distinguishable from the text.

In this work, we investigate the application of the following MPC schemes:

- LMPC,
- frozen LPVMPC,
- iterative LPVMPC,
- NMPC.

The application of these schemes onto the NL AMB system is carried out for three control problems: regulation, reference tracking and disturbance rejection. Note that, the main difference between all the considered MPC schemes, while solving the optimization problem (32), is the term $J_N(k)$ in the cost function $J(k)$ (33), which is computed during the prediction horizon N. The other terms $J_{sv}(k)$ and $J_\infty(k)$ in addition to the terminal cost are used identically in both the LPVMPC techniques and the NMPC. This is an important feature of the LPV approach, which can provide stability guarantees for NL models [29]. Moreover, we computed the required terminal ingredients for the LMPC based on a linearized LTI model of the NL system at the origin.

C. THE LMPC SCHEME

This is the standard and simplest MPC approach in terms of the computational complexity. In this scheme, we consider a discrete-time representation of a linearized model of (8) about the origin to be used over the prediction horizon in the MPC problem, thus, the cost function $J_N(k)$ in (33) is quadratic, see (34) and (35). Choosing the initial value of the states has a major effect on the feasibility of the MPC problem in this scheme, as its domain of attraction is expected to be the smallest among the other considered MPC techniques.

D. THE FROZEN LPVMPC SCHEME

In this scheme, the MPC problem is solved based on the LPV model (28). At each sampling instant k, according to the current value of the scheduling parameter, an LTI model (frozen LPV model) is computed from (28), which is used over the prediction horizon. Therefore, we refer this scheme to as frozen LPVMPC, and the cost function $J_N(k)$ is quadratic as given in (34) and (35). This procedure is repeated at every sampling instant. This scheme is similar to the LMPC one in terms of the computational complexity of the optimization problem. However, it can lead to much better performance and larger domain of attraction due to updating the model for prediction using the available value of the scheduling parameter at the time sample k.

E. THE ITERATIVE LPVMPC SCHEME

The MPC problem of this scheme is solved using the LPV model (28) with a different procedure other than that of the frozen LPVMPC. Following the approach of [27], we summarize the procedure in Algorithm 1. To simplify the representation, we use the following notations in Algorithm 1:

$$X(k) = \begin{bmatrix} x(k|k) \\ x(k+1|k) \\ \vdots \\ x(k+N-1|k) \end{bmatrix}, \quad \mathcal{M} = \begin{bmatrix} M_0 \\ M_1 \\ \vdots \\ M_{N-1} \end{bmatrix},$$

where M_i represents any of the parameter dependent matrices A_d, B_d, E_d, defined in (29) and (30), at step i of N. Note that $p(k)$ depends on $x(k)$ and $u(k)$; as a stopping criterion, we use $\|X_j(k) - X_{j-1}(k)\| < \epsilon$, where ϵ is a positive scalar, which can be chosen small enough according to the required accuracy. The frozen LPVMPC can be implemented using Algorithm 1 by skipping Steps 7-14.

Algorithm 1 Iterative LPVMPC

Require: initial state x_{ini}, x_s, u_s, N, Q or Q_y and R

1) $k \leftarrow 0$
2) $x(k) \leftarrow x_{\text{ini}}$
3) **repeat**
4)   Compute $p(k)$ using (12)
5)   Compute A_d, B_d, E_d by (29) and (30)
6)   Solve (32) to compute $U(k)$
7) $U_0(k) \leftarrow U(k)$
8) $j \leftarrow 0$
9)   **repeat**
10)   Compute $\mathcal{A}_d, \mathcal{B}_d, \mathcal{E}_d, X_j(k)$ using $U_j(k)$,(28)-(30)
11)   Solve (32) to compute $U_{j+1}(k)$
12) $j \leftarrow j+1$
13)   **until** $\|X_j(k) - X_{j-1}(k)\| < \epsilon$
14) $U(k) \leftarrow U_j(k)$
15) $u(k) \leftarrow 1^{\text{st}}$ element of $U(k)$
16)   Apply $u(k)$ on the system and obtain $x(k+1)$
17) $k \leftarrow k+1$

The main advantage of the iterative LPVMPC scheme is that it allows updating the scheduling parameter over the prediction horizon, which is more accurate than the case of the frozen scheme, thus, different LTI models can be used over N to improve the prediction in the MPC. This can lead to better performance than that of the frozen LPVMPC at the expense of extra computations and without guarantees that Steps 7-14 in Algorithm 1 will converge.

F. THE NMPC SCHEME

To solve the MPC problem here a NL discrete-time model of the AMB system is required. For simplicity, we discretize the NL model (8) using the Euler's forward method as follows

$$x(k+1) = T_s f(x, u) + x(k), \tag{44}$$

where $f(x, u)$ is given as in (9) and $T_s = 6.25 \times 10^{-4}$ s; (44) is used over the prediction horizon N to construct the cost function $J_N(k)$ in (33), which leads to a NL cost function. Therefore, to compute the optimal control input $U(k)$, the optimization problem (32) should be solved using NL optimization solvers. The optimization problem is solved at every sampling instant k. Due to the efficient description of the NL behavior of the AMB system over the prediction horizon, the NMPC scheme can achieve the best performance in comparison with the other schemes discussed above. However, the main issue, is the computational complexity associated with solving the NL optimization problem within such

high sampling rate of the system, which might be intractable in practice.

We summarize the stability result of the frozen LPVMPC scheme as follows

Theorem 1: (Asymptotically stabilizing MPC for the frozen LPV systems)

Assume there exists a terminal cost given by (37) such that (38), and (39) are satisfied, and a terminal set given by (40) such that (41) is satisfied. Consequently, the MPC controller derived by solving the optimization problem (32) can asymptotically stabilize the LPV system.

The proof of Theorem 1 follows the same lines of the work in [27].

Remark 1. Since the LPVMPC is designed based on the reduced LPV model, the theoretical stability guarantees of Theorem 1, are established for the reduced LPV model. However, in practice, due to the high accuracy of the reduced model, such guarantees can be achieved for the full model as well.

IV. SIMULATION RESULTS

In this section, the implementation of the considered MPC schemes is applied to the NL model (8) of the AMB system. To assess the operation and performance of the AMB system, we consider the following control problems:

- regulation to the origin,
- tracking a given desired reference trajectory,
- disturbance rejection,

and then we compare the proposed frozen LPVMPC with a classical lead-lag controller developed by the manufacturer of the AMB experimental setup (MBC500) [25].

Table 5 shows the considered state/input constraints, during normal operation, which cover almost the full operating range of the AMB system without exceeding the nominal air-gap ($D_0 = 4 \times 10^{-4}$ m) between the rotor and the bearing. Moreover, when the MPC optimization problem turns infeasible, we allow state constraints softening, via the slack variable, up to $1.2x_{max}$, which is still consistent with the boundary of the air-gap. It is important to satisfy the following physical condition:

$$\delta \times \dot{\delta} < 0, \quad \delta \in \{x_0, y_0, \psi, \theta\}, \quad (45)$$

on the boundaries of the state constraints initially for the successful operation of the AMB system. The simulation results considered here have been performed using QP solver [38] with YALMIP toolbox [39]. For implementing the NMPC scheme, we use the NLMPC toolbox of MATLAB R2019b.

TABLE 5. Constraints of the AMB system.

Type	Variable	Constraints
State	x_0, y_0	$-2 \times 10^{-4} - 2 \times 10^{-4}$ m
	$\dot{x}_0, \dot{y}_0$	$-0.1 - 0.1$ m/s
	ψ, θ	$-1 \times 10^{-3} - 1 \times 10^{-3}$ rad
	$\dot{\psi}, \dot{\theta}$	$-1 - 1$ rad/s
Input	$i_{x_1}, i_{x_2}, i_{y_1}, i_{y_2}$	$-1.5 - 1.5$ Amp

A. REGULATION

The control objective here is to regulate fast the state from an initial value to the origin ($x_s = 0, u_s = 0$) without violating the system constraints. We examine the feasibility of the proposed MPC schemes for different values of the initial state.

We consider initial states on the boundary of the state constraints, see Table 5, satisfying (45). By gridding the boundary, a set of initial state values has been constructed and used to test the MPC algorithms. As a representative result, we choose the initial state value $x_{ini} = [-2 \times 10^{-4}, 0.1, -2 \times 10^{-4}, 0.1, -1 \times 10^{-3}, 1, -1 \times 10^{-3}, 1]$. Next, we have operated the AMB system with all MPC schemes starting from x_{ini}. For such initial condition, all MPC approaches, except the LMPC, were successful, whereas the optimization problem of the LMPC was infeasible. Fig. 3 shows the evolution of the system state starting from x_{ini} under the frozen LPVMPC, iterative LPVMPC and NMPC, the figure indicates that these schemes can regulate the states of the AMB system within a
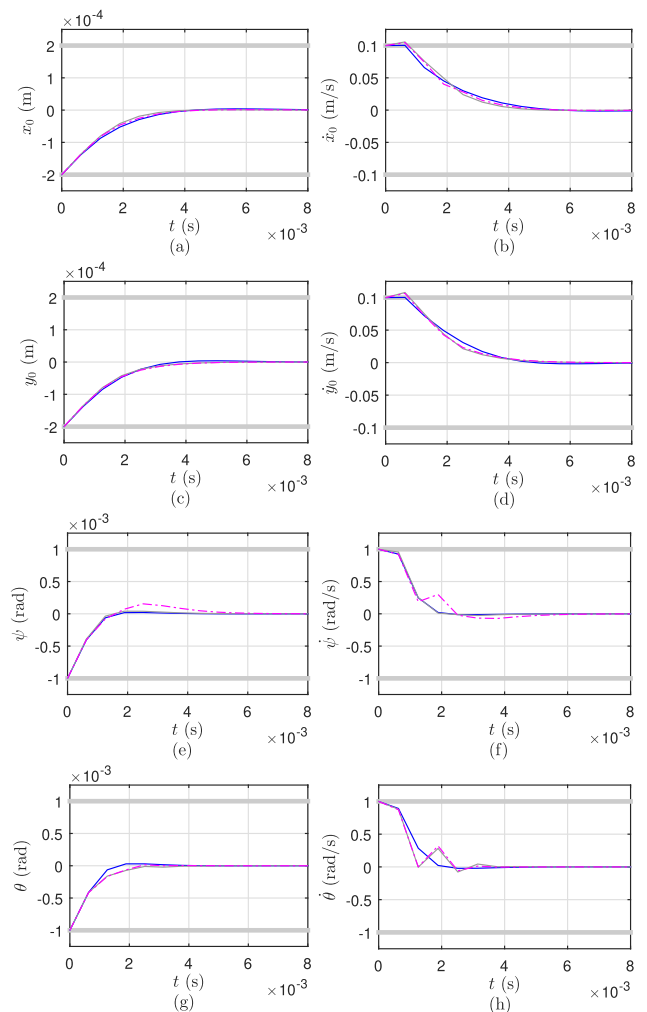

FIGURE 3. Regulation: state trajectories (NMPC —, iterative LPVMPC —, frozen LPVMPC —) and the solid gray lines represent the corresponding bounds.

short time $(2 - 6) \cdot 10^{-3}$ s without violating the constraints, however, there is some softness occurred in the constraints of the states $\dot{x}_0$ and $\dot{y}_0$, due to the activation of the slack variable $S_x(k)$, which avoids the infeasibility of the MPC optimization problem, as shown in Fig. 4. The states behavior is almost the same with the three controllers. The control inputs are shown in Fig. 5, which shows that the input constraints are satisfied.

The iterative LPVMPC scheme is, slightly, better than the frozen LPVMPC scheme and its behavior is close to the NMPC scheme, see Fig. 3(e),(f). However, in general the frozen LPVMPC scheme has achieved almost similar performance as that of the NMPC and the iterative LPVMPC schemes with less computational complexity. In case of the iterative LPVMPC, we have used $\epsilon = 10^{-8}$, which can achieve good accuracy for the stopping criterion, see Algorithm 1. It turns out that the number of iterations j, used in each sampling time for convergence was between $2 - 37$ iterations, which demonstrates its computational complexity in comparison with the frozen LPVMPC. Finally, we have observed that the LMPC scheme was not able to provide feasibility for any of the initial states considered on the boundary, whereas, all the other schemes were feasible for all considered initial state values. This can be attributed to the local behavior (close to the origin) of the LMPC scheme.
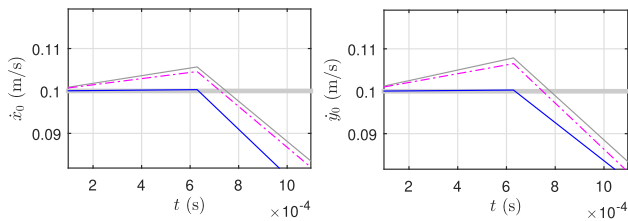

FIGURE 4. Regulation: zoomed in to trajectories of the states $\dot{x}_0$, $\dot{y}_0$ (NMPC —, iterative LPVMPC —, frozen LPVMPC —) and the solid gray lines represent the corresponding bounds.

We summarize the results of this control problem in the following points:

- The initial state x_{ini} is considered on the boundary of the state constraints.
- The LMPC optimization problem was not feasible for such initial state.
- The optimization problems of all the frozen LPVMPC, the iterative LPVMPC and the NMPC were feasible for considered initial states.
- The slack variable $S_x(k)$ has been activated shortly in all LPVMPC schemes to avoid infeasibility of the optimization problem.
- The LPVMPC and NMPC schemes successfully have regulated the states of the AMB system to the origin in a short time.
- The frozen LPVMPC has achieved almost similar performance as that of the NMPC and the iterative LPVMPC yet with less computation complexity.
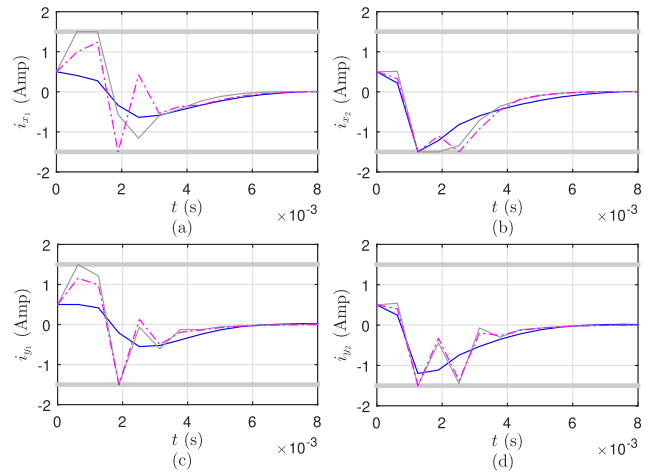- All input constraints are satisfied.

FIGURE 5. Regulation: control input trajectories (NMPC —, iterative LPVMPC —, frozen LPVMPC —) and the solid gray lines represent the corresponding bounds.

B. REFERENCE TRACKING

In this control problem, the control objective is to provide fast tracking of a reference trajectory without overshoot or steady state errors, while keeping all states and inputs of the system within their bounds. We have considered two staircase trajectories, where each one consists of two levels, this is considered as a challenging trajectory for an AMB system [21]. These levels are $\pm 1 \times 10^{-4}$ m and the duration of each level is 0.05 s, see Fig. 6. Therefore, the rotor shaft should move symmetrically around the center of the nominal air-gap, which is a challenging maneuvering as any overshoot is prohibited for the system safety.

Here, we have two steady-state values based on the considered staircase reference trajectories $x_{s_1} = [1 \times 10^{-4}, 0, -1 \times 10^{-4}, 0, 0, 0, 0, 0]$, $x_{s_2} = [-1 \times 10^{-4}, 0, 1 \times 10^{-4}, 0, 0, 0, 0, 0]$ and $u_{s_1} = [-0.13, -0.13, 0.21, 0.21]$, $u_{s_2} = [0.13, 0.13, -0.21, -0.21]$. Moreover, we have considered a new initial state $x_{\text{ini}} = [-1.2 \times 10^{-4}, 0.06, -1.2 \times 10^{-4}, 0.06, -6 \times 10^{-4}, 0.6, -6 \times 10^{-4}, 0.6]$, however, again the optimization problem of the LMPC scheme was infeasible due to its local nature (linearized around the origin). The trajectories of the outputs of the system under the frozen LPVMPC, iterative LPVMPC and NMPC are shown in Fig. 6. It shows that these controllers can efficiently yield the outputs of the AMB system on the desired staircase trajectory within $(6 - 9) \cdot 10^{-3}$ s and with almost no overshoots or steady state errors, moreover, they can deal perfectly with the coupling effects between the outputs. The corresponding control inputs are shown in Fig. 7, which satisfy their constraints. The input limits of the iterative and frozen LPVMPC were active for sometimes; however, without affecting the performance of the outputs or the stability of the system.

In this control problem, $\epsilon = 10^{-8}$ was considered again for the stopping criterion in Algorithm 1. Therefore, the iterative LPVMPC used number of iterations j ranged from 4 to 54, which indicates its computational time compared
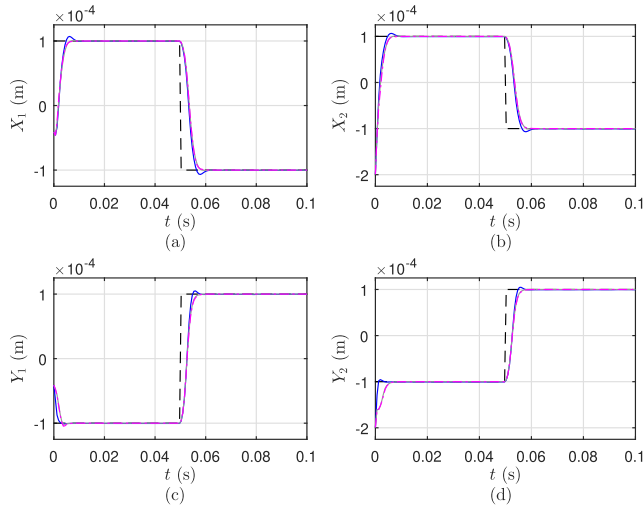
FIGURE 6. Reference tracking: output trajectories (NMPC —, iterative LPVMPC —, frozen LPVMPC —) and the dashed black lines represent the corresponding reference.

FIGURE 7. Reference tracking: control input trajectories (NMPC —, iterative LPVMPC —, frozen LPVMPC —) and the solid gray lines represent the corresponding bounds.

FIGURE 8. Disturbance rejection: output trajectories (NMPC —, iterative LPVMPC —, frozen LPVMPC —, LMPC —o) and the dashed black lines represent the corresponding reference.

to the frozen LPVMPC. Note that, the sampling time may not handle such computation burden. It is demonstrated that the most simpler and computationally efficient frozen LPVMPC scheme can achieve similar performance as that of the NMPC and the iterative LPVMPC schemes, which are more sophisticated.

The main results of the reference tracking problem are summarized as follows

- The optimization problem associated with the LMPC scheme again was not initially feasible.
- The LPVMPC and NMPC schemes showed perfect reference tracking with almost no overshoots or steady state errors and without violating the input or state constraints.
- The computational burden of the frozen LPVMPC is significantly lower than that of the iterative LPVMPC and the NMPC.

C. DISTURBANCE REJECTION

Now, we consider a disturbance f_{dist} applied on the AMB system during the reference tracking operation. An addition disturbance is applied as $\dot{x} = f(x, u) + f_{dist}$. The control objective here is to reject the effect of such disturbance within a short time without oscillations. We applied a step disturbance, as in [40], at $t = 0.02375$ s for a duration of 1.25×10^{-3} s, as shown in Fig. 8.

In this control problem, we consider $x_{\text{ini}} = 0$ and it is desired to track the constant reference $r = 1 \times 10^{-4}$ m, as shown in Fig. 8, therefore, we have one steady-state value $x_s = [1 \times 10^{-4}, 0, 1 \times 10^{-4}, 0, 0, 0, 0, 0]$ and $u_s = [-0.13, -0.13, -0.21, -0.21]$. With such scenario, the LMPC optimization problem was feasible. Fig. 8 shows the trajectories of the outputs of the system under all considered MPC schemes. In all cases the effect of the applied disturbance has been suppressed reasonably well within
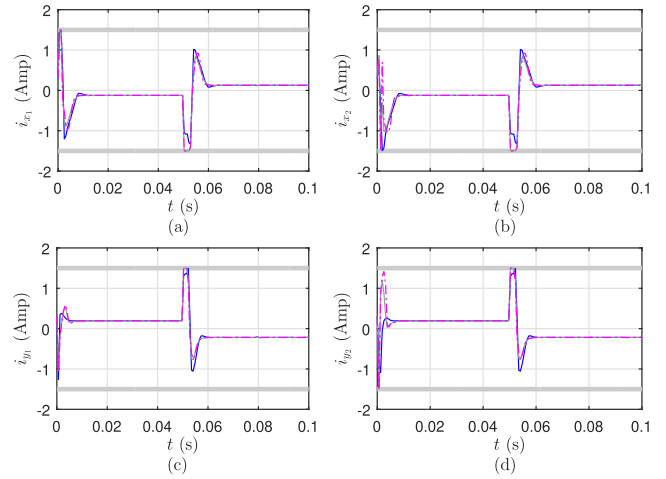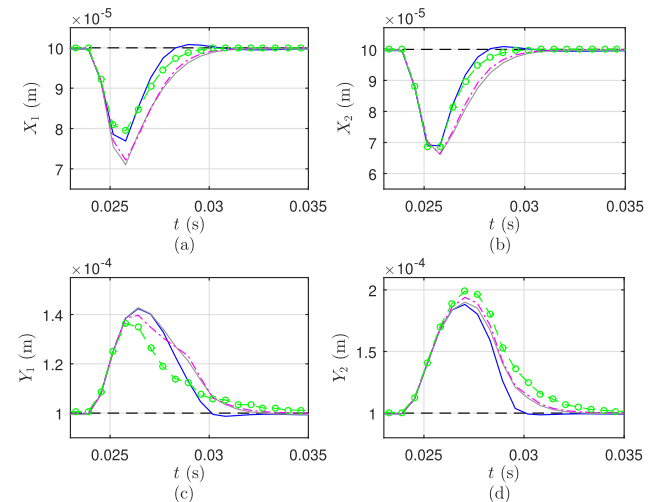
6×10^{-3} s. The state trajectories and the control inputs are shown in Figs. 9, 10, respectively. Clearly, all the MPC schemes have satisfied the input and state constraints. From Fig. 8, it is demonstrated that the performance with the LMPC scheme was reasonable; however, some of the corresponding states of the system suffer from high overshoots and oscillations as shown in Fig. 9(g),(h), moreover, some of the control input trajectories have oscillations as shown in Fig. 10(c),(d), compared with the other MPC schemes. Note that, the computation burden of the frozen LPVMPC is almost the same as that of the LMPC; however, the former one can achieve better performance for a wider range of operation.

The following points highlight the main results of this control problem:

- The optimization problem of all the MPC schemes were feasible and they were successfully able to reject
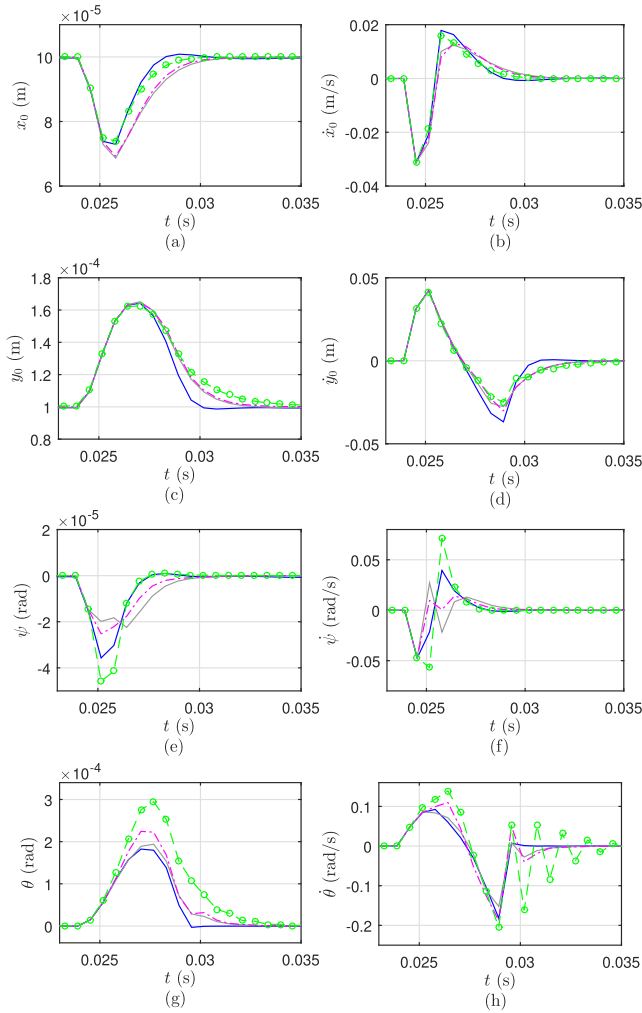
FIGURE 9. Disturbance rejection: state trajectories (NMPC —, iterative LPVMPC —, frozen LPVMPC —, LMPC —○).

FIGURE 10. Disturbance rejection: control input trajectories (NMPC —, iterative LPVMPC —, frozen LPVMPC —, LMPC —○) and the solid gray lines represent the corresponding bounds.

perfectly the applied disturbance without violating the input or the state constraints.

- At some instants, the performance of the system with the LMPC scheme suffered from high overshoots and oscillations.

D. COMPARISON WITH CLASSICAL CONTROL

In the following, we compare the performance of the proposed frozen LPVMPC scheme with a lead-lag controller, which was designed previously by the manufacturer of the AMB experimental setup (MBC500) [25]. We compare them in reference tracking. The lead-lag controller is given as

$$H_c(s) = 1.45 \frac{(1 + 0.9 \times 10^{-3}s)}{(1 + 3.3 \times 10^{-4}s)(1 + 2.2 \times 10^{-5}s)}, \quad (46)$$

which is applied onto all the outputs of the AMB system, separately. To enhance the performance of the classical controller, we have tuned its parameters according to the guidance provided in [25], which leads to the following
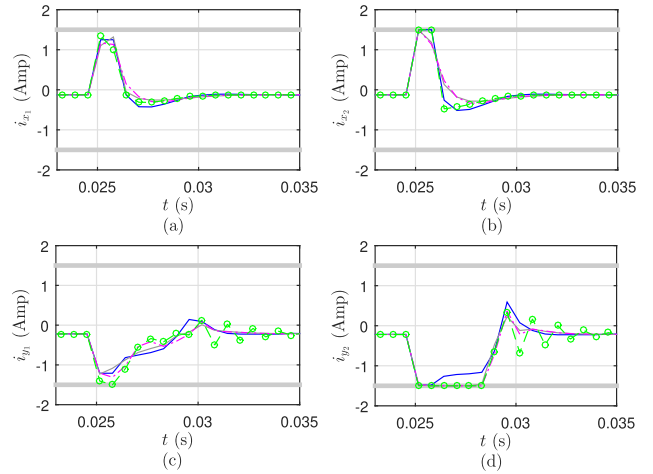
modifications:

$$C_{X_1}(s) = 18\hat{H}_c(s), \quad C_{X_2}(s) = 18\hat{H}_c(s),$$
$$C_{Y_1}(s) = 30\hat{H}_c(s), \quad C_{Y_2}(s) = 30\hat{H}_c(s), \quad (47)$$

where

$$\hat{H}_c(s) = \frac{(1 + 2 \times 10^{-3}s)}{(1 + 2.2 \times 10^{-4}s)(1 + 1.1 \times 10^{-5}s)}, \quad (48)$$

and C_{X_1}, C_{X_2}, C_{Y_1}, C_{Y_2} are the lead-lag controllers applied onto the AMB system outputs X_1, X_2, Y_1, Y_2, respectively.

Here, we considered $x_{\text{ini}} = 0$ corresponding to the nominal system, which has been used to tune the classical controller. It is worthy to mention that such classical controller cannot stabilize the system with other initial conditions. It is desired to track the staircase trajectories shown in Fig. 11. As shown
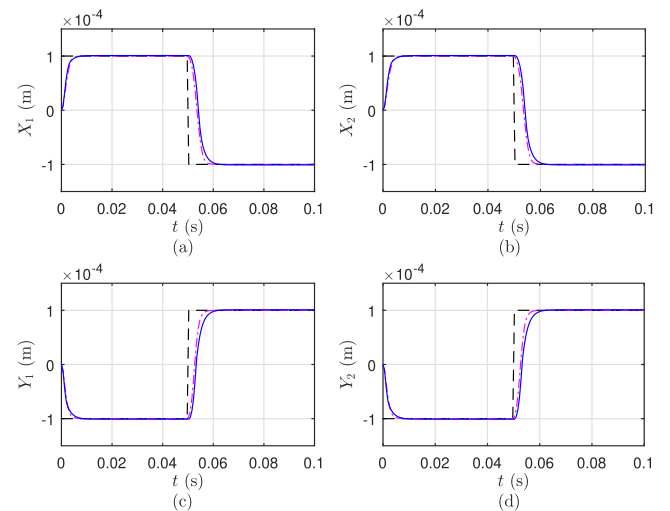

FIGURE 11. Reference tracking: output trajectories (frozen LPVMPC —, lead-lag —) and the dashed black lines represent the corresponding reference.

from the output trajectories in Fig. 11, the lead-lag controller provides almost similar performance as the frozen LPVMPC scheme, however, the input constraints at $t = (0 - 3) \cdot 10^{-3}$ s and during the transition between the two levels of the staircase reference at $t = 0.05$ s are violated as shown from the control inputs trajectories in Fig. 12. In practice, the violation of the input constraints is prohibited as it yields the AMB system in unsafe mode of operation. Moreover, the control input of the lead-lag controller suffers from some oscillations, as shown in Fig. 12(c),(d). On the other hand, the frozen LPVMPC satisfies the input constraints with perfect tracking as shown in Fig. 12.
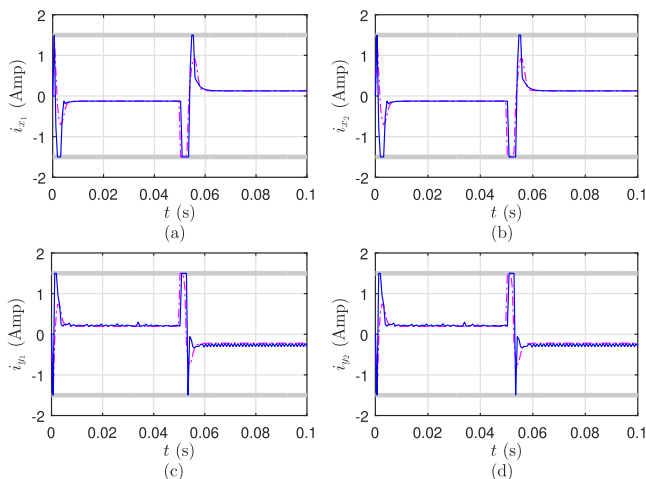

FIGURE 12. Reference tracking: control input trajectories (frozen LPVMPC $-$, lead-lag $-$) and the solid gray lines represent the corresponding bounds.

We summarize the main results of this comparison as follows

- The lead-lag controller cannot stabilize the system with any initial state other than the origin.
- The frozen LPVMPC scheme is slightly faster than the the lead-lag controller in tracking when the initial state is at the origin.
- The lead-lag controller violates the input constraints several times during the simulation, whereas, the frozen LPVMPC satisfies the input constraints.

V. CONCLUSION

The problem of controlling AMB systems based on MPC has been addressed in this paper. For tractable computation with the fast sampling rate of the system in practice, it is essential to implement a computationally cheap MPC algorithm, which at the same time can achieve high performance for a wide range of operation.

Four MPC schemes have been applied to the AMB system. The first scheme, is the conventional LMPC, which is based on a linearized model at the origin. The second one is based on an LPV model of the system where frozen scheduling parameters over the prediction horizon have been considered. The third scheme is also based on an LPV model; with an iterative

procedure to consider the variability of the scheduling parameters over the prediction horizon. Finally, the NMPC technique based on NL optimization has been considered. In order to assess the performance of these MPC schemes, three different control problems have been studied, regulation, reference tracking and disturbance rejection. In addition to that, a comparison between the frozen LPVMPC and an existent controller from practice is provided.

Stability guarantees of the considered MPC schemes are achieved via including a terminal cost and an invariant terminal set to the MPC optimization problem, which are computed offline by solving LMI problems. For tractability of these problems, the PSM technique has been used efficiently to reduce the number of the scheduling parameters without significant reduction of the accuracy of the model. To avoid infeasibility of the MPC optimization problem we include a slack variable to soften the incorporated state constraints during the execution of the MPC optimization problem.

The main message of this work is that the frozen LPVMPC strategy can achieve comparable performance to more sophisticated and computationally complex approaches, such as, the NMPC and the iterative LPVMPC schemes considered here. This will allow advanced control techniques such as MPC to be applicable for highly complex fast systems such as the AMB system.

As a next step of this work, the experimental verification of the frozen LPVMPC scheme will be carried out. Moreover, as a practical problem related to AMB systems, we will investigate the operation of the closed-loop system using MPC against imbalance sinusoidal disturbances, which is a challenging problem in practice.

APPENDIX A SCHEDULING PARAMETERS
The scheduling parameters $p_1, \ldots, p_{18}$ are computed as:

$$p_1 = a \left(\frac{1}{den_{x_1}} + \frac{1}{den_{x_2}} \right),$$

$$p_2 = al_b \left(\frac{1}{den_{x_2}} - \frac{1}{den_{x_1}} \right),$$

$$p_3 = \frac{b_2 y_1 + c_2}{den_{y_1}} + \frac{b_2 y_2 + c_2}{den_{y_2}},$$

$$p_4 = l_b \left(\frac{b_2 y_2 + c_2}{den_{y_2}} - \frac{b_2 y_1 + c_2}{den_{y_1}} \right),$$

$$p_5 = a_1 \left(\frac{1}{den_{x_2}} - \frac{1}{den_{x_1}} \right),$$

$$p_6 = a_1 l_b \left(\frac{1}{den_{x_1}} + \frac{1}{den_{x_2}} \right),$$

$$p_7 = \frac{b_3 y_2 + c_3}{den_{y_2}} - \frac{b_3 y_1 + c_3}{den_{y_1}},$$

$$p_8 = l_b \left(\frac{b_3 y_2 + c_3}{den_{y_1}} + \frac{b_3 y_2 + c_3}{den_{y_2}} \right),$$

$$p_9 = \frac{b x_1 i_{x_1} + c x_1^2 + d}{den_{x_1}},$$

$$p_{10} = \frac{bx_2 i_{x_2} + cx_2^2 + d}{den_{x_2}},$$

$$p_{11} = \frac{d_2 y_1 i_{y_1} + e_2 y_1^2 + f_2 y_1 + g_2}{den_{y_1}},$$

$$p_{12} = \frac{d_2 y_2 i_{y_2} + e_2 y_2^2 + f_2 y_2 + g_2}{den_{y_2}},$$

$$p_{13} = \frac{-b_1 x_1 i_{x_1} - c_1 x_1^2 - d_1}{den_{x_1}},$$

$$p_{14} = \frac{b_1 x_2 i_{x_2} + c_1 x_2^2 + d_1}{den_{x_2}},$$

$$p_{15} = \frac{-d_3 y_1 i_{y_1} - e_3 y_1^2 + f_3 y_1 - g_3}{den_{y_1}},$$

$$p_{16} = \frac{d_3 y_2 i_{y_2} + e_3 y_2^2 + f_3 y_2 + g_3}{den_{y_2}},$$

$$p_{17} = \frac{a_2}{den_{y_1}} + \frac{a_2}{den_{y_2}} - g,$$

$$p_{18} = \frac{a_3}{den_{y_2}} - \frac{a_3}{den_{y_1}},$$

where

$a = 4.3 \times 10^{-10}$	$a_2 = 1.3 \times 10^{-13}$
$b = 1.7 \times 10^{-9}$	$b_2 = 7.8 \times 10^{-7}$
$c = 2.1 \times 10^{-6}$	$c_2 = 1.1 \times 10^{-9}$
$d = 3.4 \times 10^{-13}$	$d_2 = 1.7 \times 10^{-9}$
$a_1 = 7.8 \times 10^{-9}$	$a_3 = 2.3 \times 10^{-12}$
$b_1 = 3.1 \times 10^{-8}$	$b_3 = 1.4 \times 10^{-5}$
$c_1 = 3.9 \times 10^{-5}$	$c_3 = 1.9 \times 10^{-8}$
$d_1 = 6.2 \times 10^{-12}$	$d_3 = 3.1 \times 10^{-8}$
$a_5 = 5 \times 10^3$	$b_5 = 25 \times 10^9$
$e_2 = 3.2 \times 10^{-6}$	$e_3 = 5.8 \times 10^{-5}$
$f_2 = 8.4 \times 10^{-10}$	$f_3 = 1.5 \times 10^{-8}$
$g_2 = 5.1 \times 10^{-13}$	$g_3 = 9.3 \times 10^{-12}$

and i_{x_i}, i_{y_i} are the system inputs, x_i, y_i are computed using (1), (2), respectively, $den_{x_i} = (x_i - 0.0004)^2 (x_i + 0.0004)^2$, $den_{y_i} = (y_i - 0.0004)^2 (y_i + 0.0004)^2$, $i = 1, 2$.

REFERENCES

[1] E. H. Maslen and G. Schweitzer, *Magnetic Bearings: Theory, Design, and Application to Rotating Machinery*. Berlin, Germany: Springer, 2009.

[2] P.-K. Budig, "Magnetic bearings and some new applications," in *Proc. IEEE Electrodyn. Mech. Syst.*, Oct. 2011, pp. 10–16.

[3] J. Kumbernuss, C. Jian, J. Wang, H. X. Yang, and W. N. Fu, "A novel magnetic levitated bearing system for vertical axis wind turbines (VAWTs)," *Appl. Energy*, vol. 90, no. 1, pp. 148–153, Feb. 2012.

[4] M. Morshuis, A. El-Banayosy, L. Arusoglu, R. Koerfer, R. Hetzer, G. Wieselthaler, A. Pavie, and C. Nojiri, "European experience of Dura-Heart magnetically levitated centrifugal left ventricular assist system," *Eur. J. Cardio-Thoracic Surg.*, vol. 35, no. 6, pp. 1020–1028, Jun. 2009.

[5] J. Ritonja, B. Polajžer, D. Dolinar, B. Grčar, and P. Cafuta, "Active magnetic bearings control," in *Proc. IEEE 29th Chin. Control Conf.*, Jun. 2010, pp. 5604–5609.

[6] C. Peng, J. Fang, and X. Xu, "Mismatched disturbance rejection control for voltage-controlled active magnetic bearing via state-space disturbance observer," *IEEE Trans. Power Electron.*, vol. 30, no. 5, pp. 2753–2762, May 2015.

[7] A. M. Mohamed and I. Busch-Vishniac, "Imbalance compensation and automation balancing in magnetic bearing systems using the Q-parameterization theory," *IEEE Trans. Control Syst. Technol.*, vol. 3, no. 2, pp. 202–211, Jun. 1995.

[8] A. M. Mohamed, F. Matsumura, T. Namerikawa, and J.-H. LeeHJun, "Modeling and robust control of self-sensing magnetic bearings with unbalance compensation," in *Proc. IEEE Int. Conf. Control Appl.*, 1997, pp. 586–594.

[9] C. Liu, G. Liu, and J. Fang, "Feedback linearization and extended state observer-based control for rotor-AMBs system with mismatched uncertainties," *IEEE Trans. Ind. Electron.*, vol. 64, no. 2, pp. 1313–1322, Feb. 2017.

[10] X. Yao, Z. Chen, and Y. Jiao, "A dual-loop control approach of active magnetic bearing system for rotor tracking control," *IEEE Access*, vol. 7, pp. 121760–121768, 2019.

[11] K.-Y. Chen, P.-C. Tung, M.-T. Tsai, and Y.-H. Fan, "A self-tuning fuzzy PID-type controller design for unbalance compensation in an active magnetic bearing," *Expert Syst. Appl.*, vol. 36, no. 4, pp. 8560–8570, May 2009.

[12] Y. Wang, Y. Chang, A. F. Alkhateeb, and N. D. Alotaibi, "Adaptive fuzzy output-feedback tracking control for switched nonstrict-feedback nonlinear systems with prescribed performance," *Circuits, Syst., Signal Process.*, vol. 40, pp. 88–113, Jan. 2021.

[13] L. Ma, G. Zong, X. Zhao, and X. Huo, "Observed-based adaptive finite-time tracking control for a class of nonstrict-feedback nonlinear systems with input saturation," *J. Franklin Inst.*, vol. 357, no. 16, pp. 11518–11544, Nov. 2020.

[14] J. M. Maciejowski, *Predictive Control: With Constraints*. London, U.K.: Pearson Education, 2002.

[15] A. Morsi, H. S. Abbas, and A. M. Mohamed, "Wind turbine control based on a modified model predictive control scheme for linear parameter-varying systems," *IET Control Theory Appl.*, vol. 11, no. 17, pp. 3056–3068, Nov. 2017.

[16] U. R. Nair and R. Costa-Castelló, "A model predictive control-based energy management scheme for hybrid storage system in islanded microgrids," *IEEE Access*, vol. 8, pp. 97809–97822, 2020.

[17] B. Kouvaritakis and M. Cannon, *Model Predictive Control Classical, Robust Stochastic*. Cham, Switzerland: Springer, 2016.

[18] W. J. Rugh and J. S. Shamma, "Research on gain scheduling," *Automatica*, vol. 36, no. 10, pp. 1401–1425, Oct. 2000.

[19] H. S. Abbas, A. Ali, S. M. Hashemi, and H. Werner, "LPV state-feedback control of a control moment gyroscope," *Control Eng. Pract.*, vol. 24, pp. 129–137, Mar. 2014.

[20] S. Mate, H. Kodamana, S. Bhartiya, and P. S. V. Nataraj, "A stabilizing sub-optimal model predictive control for quasi-linear parameter varying systems," *IEEE Control Syst. Lett.*, vol. 4, no. 2, pp. 402–407, Apr. 2020.

[21] J. Huang, L. Wang, and Y. Huang, "Continuous time model predictive control for a magnetic bearing system," *PIERS Online*, vol. 3, no. 2, pp. 202–208, 2007.

[22] K. R. Uren, G. van Schoor, and C. D. Aucamp, "Model predictive control of an active magnetic bearing suspended flywheel energy storage system," *SAIEE Afr. Res. J.*, vol. 106, no. 3, pp. 141–151, Sep. 2015.

[23] L. Papini, L. Tarisciotti, A. Costabeber, C. Gerada, and P. Wheeler, "Active magnetic bearing system design featuring a predictive current control," in *Proc. 42nd Annu. Conf. IEEE Ind. Electron. Soc. (IECON)*, Oct. 2016, pp. 3217–3222.

[24] A. Morsi, H. S. Abbas, S. M. Ahmed, and A. M. Mohamed, "Model predictive control for an active magnetic bearing system," in *Proc. IEEE 7th Int. Conf. Ind. Eng. Appl. (ICIEA)*, Apr. 2020, pp. 715–720.

[25] N. Morse, R. Smith, and B. Paden, "Magnetic bearing lab# 1: Analytical modeling of a magnetic bearing system," Comput. Math. Appl., Magn. Moments LLC, Goleta, CA, USA, Tech. Rep., 1996.

[26] A. Kwiatkowski and H. Werner, "PCA-based parameter set mappings for LPV models with fewer parameters and less overbounding," *IEEE Trans. Control Syst. Technol.*, vol. 16, no. 4, pp. 781–788, Jul. 2008.

[27] P. S. G. Cisneros, S. Voss, and H. Werner, "Efficient nonlinear model predictive control via quasi-LPV representation," in *Proc. IEEE 55th Conf. Decis. Control (CDC)*, Dec. 2016, pp. 3216–3221.

[28] D. Q. Mayne, J. B. Rawlings, C. V. Rao, and P. O. M. Scokaert, "Constrained model predictive control: Stability and optimality," *Automatica*, vol. 36, no. 6, pp. 789–814, Jun. 2000.

[29] C. Hoffmann and H. Werner, "A survey of linear parameter-varying control applications validated by experiments or high-fidelity simulations," *IEEE Trans. Control Syst. Technol.*, vol. 23, no. 2, pp. 416–433, Mar. 2015.

[30] J. Hanema, M. Lazar, and R. Tóth, "Stabilizing tube-based model predictive control: Terminal set and cost construction for LPV systems," *Automatica*, vol. 85, pp. 137–144, Nov. 2017.

[31] H. S. Abbas, G. Männel, C. Herzog Né Hoffmann, and P. Rostalski, "Tube-based model predictive control for linear parameter-varying systems with bounded rate of parameter variation," *Automatica*, vol. 107, pp. 21–28, Sep. 2019.

[32] F. Blanchini and S. Miani, *Set-Theoretic Methods in Control*. Boston, MA, USA: Birkhäuser, 2008.

[33] J. B. Rawlings and D. Q. Mayne, *Model Predictive Control: Theory Design*. Madison, WI, USA: Nob Hill, 2009.

[34] S. M. Hashemi, H. S. Abbas, and H. Werner, "Low-complexity linear parameter-varying modeling and control of a robotic manipulator," *Control Eng. Pract.*, vol. 20, no. 3, pp. 248–257, 2012.

[35] J. E. Jackson, *A User's Guide to Principal Components*, vol. 587. Hoboken, NJ, USA: Wiley, 2005.

[36] H. S. Abbas, J. Hanema, R. Tóth, J. Mohammadpour, and N. Meskin, "An improved robust model predictive control for linear parameter-varying input-output models," *Int. J. Robust Nonlinear Control*, vol. 28, no. 3, pp. 859–880, Feb. 2018.

[37] C. T. Kelley, *Solving Nonlinear Equations With Newton's Method*. Philadelphia, PA, USA: SIAM, 2003.

[38] K.-C. Toh, M. J. Todd, and R. H. Tütüncü, "SDPT3—A MATLAB software package for semidefinite programming, version 1.3," *Optim. Methods Softw.*, vol. 11, nos. 1–4, pp. 545–581, 1999.

[39] J. Lofberg, "YALMIP: A toolbox for modeling and optimization in MATLAB," in *Proc. IEEE Int. Conf. Robot. Autom.*, Sep. 2004, pp. 284–289.

[40] A. Noshadi, J. Shi, W. S. Lee, P. Shi, and A. Kalam, "Robust control of an active magnetic bearing system using H_∞ and disturbance observer-based control," *J. Vib. Control*, vol. 23, no. 11, pp. 1857–1870, 2017.

HOSSAM SEDDIK ABBAS received the B.Sc. and M.Sc. degrees from Assiut University, in 1997 and 2001, respectively, and the Ph.D. degree from the Hamburg University of Technology, Germany, in 2010. He is affiliated as a Professor with the Electrical Engineering Department, Faculty of Engineering, Assiut University, Egypt, where he has been an Associate Professor and an Assistant Professor from 2015 to 2020 and from 2010 to 2015, respectively. He is currently a Senior Scientist with the Institute for Electrical Engineering in Medicine, Universität zu Lübeck, Germany. In 2019, he worked in the Medical Laser Centre Lübeck, Germany, as a Senior Scientist. From 2017 to 2019, he was an Alexander-von-Humboldt Fellow (Georg Forster Research Fellowship for Experienced Researchers) with the Institute for Electrical Engineering in Medicine, Universität zu Lübeck, Germany. He was a Research Fellow with the Hamburg University of Technology, and Eindhoven University of Technology, The Netherlands, in 2011 and 2013, respectively. His research interests include the area of control systems engineering and its applications. His focus includes linear parameter varying systems, optimal and robust control, model predicative control, distributed control, and system identification.

SABAH MOHAMED AHMED was born in Assiut, Egypt, in 1956. She received the B.Sc.E.E. (Hons.) and M.Sc.E.E. degrees in electrical engineering from Assiut University, Egypt, in 1979 and 1985, respectively, and the Ph.D. degree from the Technical University of Budapest, Hungry, in 1992. She worked at the Faculty of Engineering, Assiut University, as a Demonstrator, in 1979, an Assistant Lecturer, in 1985, an Assistant Professor, in 1992, an Associate Professor, in 2002, and a Professor, in 2009. She joined the Electronics Engineering Department, Hijjawi Faculty for Engineering Technology, Yarmouk University, in 1996, Jordan, Jarash Private University, in 1997, Jordan, and Computer Science Department, Zarka Private University, in 2000, Jordan, as a Visiting Professor. Her research interests include Speech analysis and synthesis, digital filters, biomedical signal processing, data compression, wavelet-transforms, genetic and immune algorithms, and mechatronics and robotics. She authored or coauthored over 60 published articles in the above fields. She is currently a Professor with the Mechatronics and Robotics Engineering Department, School of Innovative Design Engineering, Egypt-Japan University of Science and Technology (E-JUST), Egypt, since August 2017.

ABDELFATAH MAHMOUD MOHAMED (Life Senior Member, IEEE) received the Ph.D. degree from the University of Maryland, College Park, USA, in 1990. Since 1990, he has been an Assistant Professor with the Electrical Engineering Department, Assiut University, Egypt. He became an Associate Professor, in 1995, and a Professor, in 2000. From September 1990 to August 1993, he was a Postdoctoral Fellow with the Mechanical Engineering Department, University of Texas, Austin, USA. From April 1996 to April 1997, he was a Visiting Professor with the Electrical Engineering Department, Kanazawa University, Japan. From September 2010 to March 2012, he was the Head of the Electrical Engineering Department, Assiut University, and became the Dean of Faculty of Engineering, Assiut University, in March 2012. From November 2013 to September 2018, he was the Head of the Mechatronics and Robotics Engineering Department, School of Innovative Design Engineering, Egypt-Japan University of Science and Technology (E-JUST), Egypt, and, he is currently an Emirates Professor. His research interests include robust and intelligent control, magnetic bearing systems, robotics, and industrial drives.

ABDELRAHMAN MORSI was born in Assiut, Egypt, in November 1989. He received the B.Sc. and M.Sc. degrees from the Electrical Engineering Department, Faculty of Engineering, Assiut University, Egypt, in 2011 and 2016, respectively. He is currently pursuing the Ph.D. with the Mechatronics and Robotics Engineering Department, School of Innovative Design Engineering, Egypt Japan University of Science and Technology (E-JUST), Egypt. He is also affiliated with the Electrical Engineering Department, Faculty of Engineering, Assiut University, since 2011. His current research interests include automatic control, linear parameter varying systems, model predictive control, and magnetic bearing systems.

• • •